Compression of spin-polarized hydrogen bubbles to thermal explosion

T. Tommila, E. Tjukanov, M. Krusius,* and S. Jaakkola
Department of Physical Sciences and Wihuri Physical Laboratory, University of Turku, 20500 Turku, Finland
(Received 2 February 1987; revised manuscript received 1 June 1987)

We have compressed spin-polarized atomic hydrogen gas in small, $\gtrsim 10^{-6}$-cm^3 bubbles to densities higher than 10^{18} cm^{-3} using a liquid-^{4}He piston at temperatures from 0.3 to 0.7 K and in magnetic fields from 4.5 to 7.5 T. A best fit to the compression sweeps is obtained by fixing the binding energy of the adsorbed H atom on the liquid ^{4}He surface to 1.15 K, which then yields the third-order dipolar recombination rate constants $K^v_{bbb}=2.7(7)\times 10^{-39}$ cm^6/s for the gas phase and $K^s_{bbb}=8(2)\times 10^{-25}$ cm^4/s for the adsorbed surface layer. Because of inadequate transfer of the recombination heat to the surrounding He bath, the compression sweeps terminate in a spontaneous thermal explosion of the H↓ bubble. The pressure at the onset of the explosive recombination event is investigated as a function of ambient temperature, bubble volume, and magnetic field. Qualitative agreement with a simple thermally activated explosion model is found.

I. INTRODUCTION

Spin-polarized atomic hydrogen (H↓) was first stabilized[1] to a density of about $n=10^{14}$ cm^{-3} and later to about $n=10^{17}$ cm^{-3} by straightforward loading of the H↓ sample cell with an intense H atom flux from a H_2 dissociator. Beyond that, densities in excess of 10^{18} cm^{-3} have only been achieved[2-7] by compression techniques. However, even these attempts have not proved adequate for reaching the Bose-Einstein condensed (BEC) state of this weakly interacting boson gas[8,9] at temperatures below 1 K and in magnetic fields B of order 10 T. The H↓ atom flux to the sample cell contains, initially, atoms in both the two lowest (electronically polarized) hyperfine states $|a\rangle \simeq -|{\downarrow}{\ddagger}\rangle+\epsilon|{\uparrow}{\ddagger}\rangle$ and $|b\rangle=|{\downarrow}{\ddagger}\rangle$, where ↓ and ↑ denote the electron spin, ‡ and ‡ the nuclear spin, and ϵ is the hyperfine mixing parameter $\epsilon\approx(0.0253\ \mathrm{T})/B$. In a collision of two atoms in the pure $|b\rangle$ state the electronic H-H singlet character is not available, but in atomic collisions $|a\rangle+|a\rangle$ and $|a\rangle+|b\rangle$ the formation of the binding singlet state and consequent recombination to a H_2 molecule is possible with a probability proportional to ϵ^2. These second-order recombinations (respectively, to para-H_2 and ortho-H_2) limit the ultimate density in the H↓ cell during loading to 10^{16}–10^{17} cm^{-3}. When the H flux is turned off, recombination gradually depletes the $|a\rangle$ state population until one is left with a sample composed almost entirely of doubly polarized $|b\rangle$ state atoms. At this point recombination is impeded by the slow nuclear relaxation from the $|b\rangle$ level to the ground state $|a\rangle$,[10] which in terms of respective rate constants may be expressed as $G_{ba}\ll K^{\mathrm{eff}}_{aa}, K^{\mathrm{eff}}_{ab}$. This means that the nuclear polarization, defined as

$$M=(n_b-n_a)/(n_b+n_a)-(n_b-n_a)/n\ ,$$

grows spontaneously with time, and values $M>98\%$ have been observed.[11,12]

More elevated H↓ densities can at high polarization M be produced by compressing the double-polarized gas in a closed volume. So far densities up to $n\approx 5\times 10^{18}$ cm^{-3} have been reported for samples confined at $T\approx 0.6$ K to superfluid liquid-^{4}He-lined cells and compressed by raising the He-bath level by either displacing liquid with a plunger[2-5] or by hydraulic actuation of a bellows assembly.[6,7] Yet these densities are decisively short of the BEC limit $n_{\mathrm{BEC}}\simeq 2.3\times 10^{20}$ cm^{-3} for 0.6 K [$n_{\mathrm{BEC}}=(mk_BT/3.31\hbar^2)^{3/2}$]. There seem to be two foremost obstacles to the achievement of BEC in compressed H↓: First, at $n\gtrsim 10^{17}$ cm^{-3}, electromagnetic interactions between three H↓ atoms,[13,14] even if all three H↓ atoms are in the $|b\rangle$ state, become the dominant cause of electronic triplet-singlet transitions. The third-order recombination processes take place both in the bulk gas and in the H↓ overlayer adsorbed on the confining walls. Thus the recombination rate separates into volume (v) and surface (s) parts:

$$-\dot{N}/V=K_3n^3=K^v_3n^3+(A/V)K^s_3n_s^3\ , \tag{1}$$

where A is the surface area, V the sample volume, and n_s the H↓ surface density. In the low-density limit (e.g., $n<10^{18}$ cm^{-3} at $T>0.3$ K on a ^{4}He surface; cf. Refs. 8, 9, and 15) n_s is given by the classical adsorption isotherm,

$$n_s=n\lambda_T\exp(E_a/k_BT)\ , \tag{2}$$

where E_a is the adsorption energy and $\lambda_T=(2\pi\hbar^2/mk_BT)^{1/2}$ is the thermal de Broglie wavelength of a H particle. According to Eqs. (1) and (2) it is obvious that towards low temperatures, where lower densities would be needed for the BEC, surface recombination will increase exponentially, while at higher temperatures bulk processes are the more stringent limitation to the lifetime and ultimate density of the sample.

The most analyzed third-order recombination process proceeds via the electronic dipole mechanism.[13] It becomes effective when two H atoms to be recombined experience different magnetic field fluctuations due to pair-

wise electron dipole-dipole interaction with a third H atom. Third-order mechanisms are mediated also by exchange interactions.[13,14] As opposed to second-order processes, where a third particle or the surface is needed only to conserve energy and momentum, the third H↓ atom plays an active role in third-order recombinations. It has a high probability to become spin-flipped to the state $|c\rangle \simeq |\uparrow\downarrow\rangle + \epsilon |\downarrow\downarrow\rangle$ and recombined promptly with a fourth atom. Another depolarising channel is the two-body electronic $|b\rangle \rightarrow |c\rangle$ relaxation[2,13] across the $2\mu_B B$ Zeeman splitting. This thermally activated process operates in the bulk gas at the rate $G_{cb}^{v} \exp(-2\mu_B B/k_B T) n^2$, which becomes noticeable only for $B/T < 10$ T/K. Thus the stability of H↓ against electronic relaxation is strongly enhanced by operating in a higher magnetic field. The third-order rate constants of Eq. (1) have been observed[5,16] to decrease slightly with B, contrary to theoretical results[13] (see, however, Ref. 14).

The second main barrier against achieving BEC in dense H↓ is the poor transfer of recombination heat ($H+H \rightarrow H_2 + D$ where $D = 4.48$ eV per H_2 molecule) to the walls of the sample. Due to the finite thermal conductivity of the viscous H↓ gas[17] and the Kapitza thermal boundary resistance across the gas-liquid He interface,[18] enough heat cannot escape from the sample, which thus will be driven out of thermal equilibrium. If the recombination rate increases with increasing temperature, the highly exothermic reaction kinetics may ultimately trigger a thermal runaway which proceeds in an explosive manner. Thermal explosions in H↓ were predicted by Stwalley *et al.*,[19] and were first observed by Sprik *et al.*[2] and modeled by Kagan *et al.*[20] In this paper we describe compression experiments with small H↓ bubbles imbedded in bulk liquid helium at temperatures between about 0.3 and 0.7 K in fields $B = 4.5-7.5$ T. As in our earlier shorter reports[6,7] the emphasis is on a systematic study of the onset conditions for the thermal explosions and on the implications of the explosions to the attainment of phase transitions in H↓. The experimental apparatus and measuring procedure as well as a thermal explosion model are next described in some detail. The extraction of the third-order recombination rate constants from volume decay data is also presented.

II. APPARATUS

A coaxial and tunable $\lambda/4$ cavity resonator operated at 2.45 GHz is used for dissociating H_2 molecules in a 0.3-cm-i.d. fused-quartz discharge tube. A flow of purified H_2 at about 1 Torr is fed to this dissociator, located on the top of the cryostat, while it is cooled with water and air flows. In order to attain a high dissociation degree, the tuning of the cavity is checked by monitoring the intensity of the red H_α line in the discharge light. From the dissociator a H-atom flux of $(5-8)\times 10^{17}$ H atoms/s effuses into a 170-cm-long tube assembly along which the atoms are transported down to the sample cell. In order to avoid excessive losses from surface recombination, the transport tube is coated with materials on which hydrogen atoms have as low a sticking probability and adsorption energy as possible.

The atoms first effuse from the discharge tube through a 0.4-mm-diam orifice into a 120-cm-long, 0.8-cm-i.d. $\times$ 0.05-cm wall Teflon tube inserted in a 1.0-cm-i.d. vacuum-insulated stainless-steel tube. The Teflon tube is maintained at temperatures above 20 K with a heater wound around the lower half of the tube. The latter fits into a short nylon tube which forms a transition region,[21] where H atoms are rapidly thermalized to liquid-helium temperatures by collisions with refrigerated walls, but where a superfluid ^{4}He film cannot yet be maintained. In this region the recombination losses pile up and the surfaces acquire a solid H_2 coating, which reduces the adsorption energy for H. Nevertheless, surface recombination on the radiation baffle at the outlet of the Teflon tube and in the nylon tube is the predominant cause for the total transport loss of more than 3 orders of magnitude. The nylon part exposed to H is only 2 cm long with a 0.5-cm-i.d. $\times$ 0.03-cm wall. A separate heater wire is wound around the nylon tube.

The lower end of the nylon tube is fixed to a 1.6-cm high and 1.2-cm-i.d. copper vessel, called the film reservoir (FR),[21] which is connected to a recirculating ^{3}He refrigerator having an effective cooling power of 3 mW at 0.6 K. The refrigerator maintains the temperature of the FR below 0.85 K in order to keep the ^{4}He vapor pressure low enough such that a superfluid film prevails on the walls of the FR and the volume recombination rate remains at an acceptable level. A sintered copper heat exchanger on the bottom of the FR not only enhances heat transfer to the ^{3}He pot, but also creates a storage for liquid He to replenish the superfluid film coating at spots on the FR wall possibly bared by recombination. As excessive cooling of the nylon and Teflon tubes should be avoided, the temperature of the FR cannot be lowered below a certain threshold. As described in more detail in Ref. 21, the H atom transparency of the transport tube critically depends on the temperature profile of this section of the H fill line. From the FR hydrogen, atoms are guided into the sample cell (SC), located 46 cm below the FR, through superfluid-film-lined metal (Cu-Ni and Cu) tubes. This section is weakly thermally anchored to the mixing chamber, and its flow impedance is large enough to preclude excessive cryopumping and consequent depletion of the film in the FR and an intolerable deposition of He condensation heat on the SC from the refluxing He gas stream.

Two different SC's have been used in this work to confine H↓ atoms in the center of an 8-T and 7.0-cm-bore superconducting magnet. Both cell bodies were made of high purity copper and are connected to the mixing chamber of a homemade dilution refrigerator[22] by four 0.6-cm-diam and 20-cm-long copper rods (see Fig. 1). The thermal impedance of this connection is $\Delta T/Q \approx (90/T)$ K^2/W. With a 0.4-mmol/s circulation the cooling power of the mixing chamber is 0.8 mW at 0.3 K. In both cells the sample is analyzed in a flat cylindrical volume between two Kapton foils. However, in the larger cell[6] this analyzing space (AS) is 0.087(5) cm high and 2.0 cm in diameter, while in the smaller SC, depicted in Fig. 1, the AS is 0.022(1) cm high (thickness of

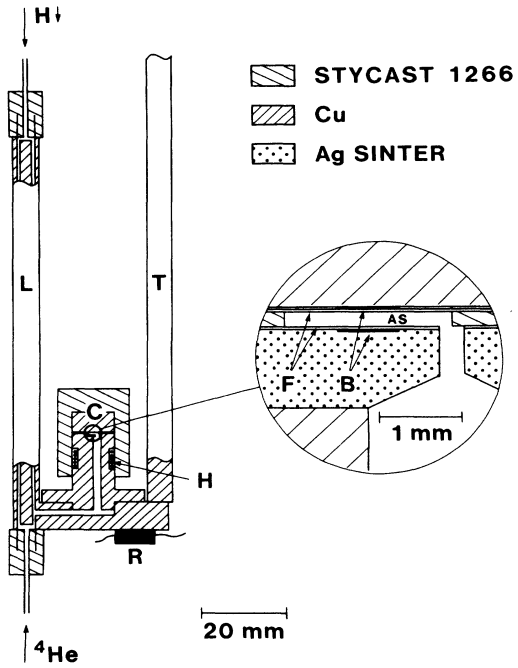

FIG. 1. The smaller sample cell for compression experiments on H↓. The analyzing space AS (inset) inside the cell body C is 2 mm in diameter and bounded by two gold-evaporated Kapton foils F and a 0.22 mm thick epoxy spacer. The outer leg L is a coaxial capacitive level indicator for liquid helium, T represents one of four thermal contact rods to the mixing chamber, H represents the heater, R the carbon resistance thermometer, and B the thin carbon (Aquadag) bolometers.

the epoxy spacer) and 0.2 cm in diameter. The majority of the compression experiments has been carried out with the latter SC. The gold-evaporated inward-facing surfaces of the Kapton foils served as the electrodes of a capacitive volume gauge. The sample volume V is determined from the amount of liquid helium displaced by the H↓ bubble in this plate capacitor. The relative dielectric constant of liquid ^{4}He is taken to be 5.7% larger than that of vacuum (H↓).[3] The gauge capacitor is connected to a bridge circuit including a 1-kHz, 20-V stable signal generator, a seven-decade ratio transformer standard, and a lock-in amplifier. The smallest detectable volume V is about 10^{-5} cm^3 in the large SC and 10^{-6} cm^3 in the small SC.

An appendage to the SC in the form of a coaxial capacitor provides a liquid helium level gauge for the measurement of the hydrostatic pressure head, P_h, above the AS. In the small SC (Fig. 1) the level gauge acts also as the lowermost part of the H↓ filling tube. The capacitor is part of a tunnel-diode oscillator circuit[23] operating at 17 MHz with a sensitivity of -1.7 kHz/(mm^{4}He) (1 mm^{4}He$=1.43$ Pa). The oscillator is connected to a precision frequency counter. The resolution of the level gauge is 0.02 mm, when the liquid meniscus is at rest in the 0.05-cm-wide capacitor annulus. In nonstationary situations the resolution depends on the time constants of the electronic circuit and the advance rate of the meniscus in the annulus. The zero of the gauge is aligned with the abrupt change of the rate of the level rise when the level passes from the large horizontal reservoir space of the SC to the 2.00(1)-cm-high, 0.2-cm-diam volume leading to the AS. The calibration of the level reading is obtained from the active length 9.80(5) cm of the gauge capacitor.

The ambient temperature T_0 in the SC is measured with a 0.1×0.1-cm^2 carbon film bolometer located on the outward side of the upper Kapton foil (Fig. 1). The bolometer has been made by painting a thin layer of colloidal graphite (Aquadag, particle size about 1 μm) between evaporated gold contact strips. The temperature calibration[22] is based on a NBS fixed-point device (SRM 768) in the low-temperature regime and on a calibrated Ge temperature sensor at temperatures above 1.5 K. A magnetic La-diluted cerium-magnesium-nitrate thermometer is calibrated against these standards and is then used to calibrate another magnetically shielded Ge resistor. Finally the bolometer is calibrated in different magnetic fields against this latter Ge resistor. To guarantee good thermal contact between the bolometer and the cell body during calibration, the AS is filled with liquid ^{4}He. We estimate the error in our calibration to be less than 5%. The bolometer can record short transient heat pulses released in an explosive recombination blast of about 10^{12} or more H↓ atoms. To improve thermal contact between the cell body and liquid helium a silver sinter with a surface area of roughly 800 cm^2 is located below the lower Kapton foil.

A hydraulic liquid-He driven device[6] is used with which liquid helium can be raised to the SC in order to close it off, to change its volume, and finally to compress the H↓ sample into a bubble in the top part of the SC. Beneath the SC there are two concentric bronze bellows: During pressurization the inner bellows expands whereas the outer bellows contracts and transfers liquid to the SC. The outer bellows contains 30 cm^3 liquid helium, of which about 10% can be raised to the SC and the level indicator. The drive pressure, up to about 4 bars, is transmitted from the outside of the cryostat to the inner bellows and is regulated with a needle valve system that makes extremely small compression rates possible.

III. OPERATING PROCEDURES

After the transport tube and the SC have been stabilized to their respective temperatures, accumulation of hydrogen atoms from the glow discharge to the SC is started. When a density 10^{14}–10^{16} cm^{-3} is achieved, the compression device is actuated to raise liquid helium from the outer bellows to the level where it just closes off the H↓ inlet and stops the accumulation. By further elevating the ^{4}He level the sample is pressurized to a higher density. An important characteristic of the compression experiment is the fact that when the liquid rises closer to the AS, the thickness of the film on the walls of the AS increases up to approximately 10 μm, which is thick enough[24] to shield off possible magnetic impurities which cause first-order recombination. Next liquid ^{4}He enters the AS in a surge pushed by capillary

action through the 0.032(2)-cm-diam hole in the sinter (Fig. 1), which causes the newly formed H↓ bubble to oscillate. In a couple of seconds the bubble relaxes to a stable disk, which then shrinks horizontally inside the AS until it becomes small enough to lose contact with the lower foil and to attain nearly spherical shape. When the liquid level rises in the filling tube, the gas pressure in the bubble increases further. The compression is done relatively slowly to allow $|a\rangle$ state atoms to recombine so that a high steady-state nuclear polarization is reached well prior to any explosion [see Fig. 7(b)].

During the compression sweep some H↓ gas stays at low pressure in the high-field region of the filling tube. It is possible to refill the SC, sometimes even five times, with these atoms by lowering the liquid helium level to open the H↓ inlet.[6] In this way samples with initially less and less atoms can be produced.

Figure 2 illustrates the final stage of a typical compression sweep. Chart recorder traces for the ambient temperature T_0, the volume V, and the hydrostatic pressure P_h are shown. Before reaching this stage the H↓ sample has been compressed typically for 5–10 s after closing the inlet. Due to the relatively low initial densities the polarization does not increase much during this time from its initial value $M \simeq 0$. Constant compression speeds of 0.3–7 Pa/s have been used once the sample is inside the AS. The steps in the level gauge signal are due to the finite counting time of the frequency counter. The bubble explodes at the moment when there appears a steep spike in the bolometer signal and the volume signal suddenly drops to zero. The time constant of the volume measurement is 30 ms.

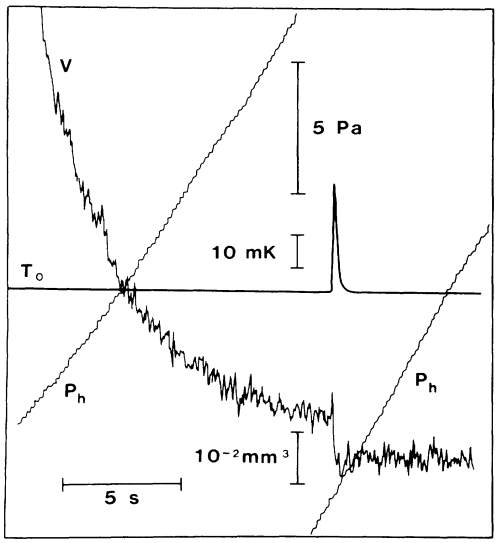

FIG. 2. Recorder traces of a compression sweep at ambient (bolometer) temperature $T_0 = 0.53$ K in a 7.5 T field. The thermal explosion manifests itself as a spike in the bolometer signal and an abrupt decrease of the volume gauge signal (V). The linear compression drive is represented by the level indicator signal (P_h).

In order to check our pressure and volume measurement compression-decompression cycles were made[25] on H↓ in the AS of the small SC at different temperatures. In this case the bubble was not compressed to the explosion limit. It could be decompressed by pumping on the primary bellows of the pressurizing device through a needle valve. The oscillating hydrostatic pressure P_h and the volume V are shown in Fig. 3(a) during a typical compression-decompression experiment. Because the densities are low ($< 10^{18}$ cm^{-3}), we can apply the ideal gas law to calculate the total number of atoms $N = PV/k_B T$. The temperature T inside the bubble can be assumed to stay fairly close to the ambient tempera-

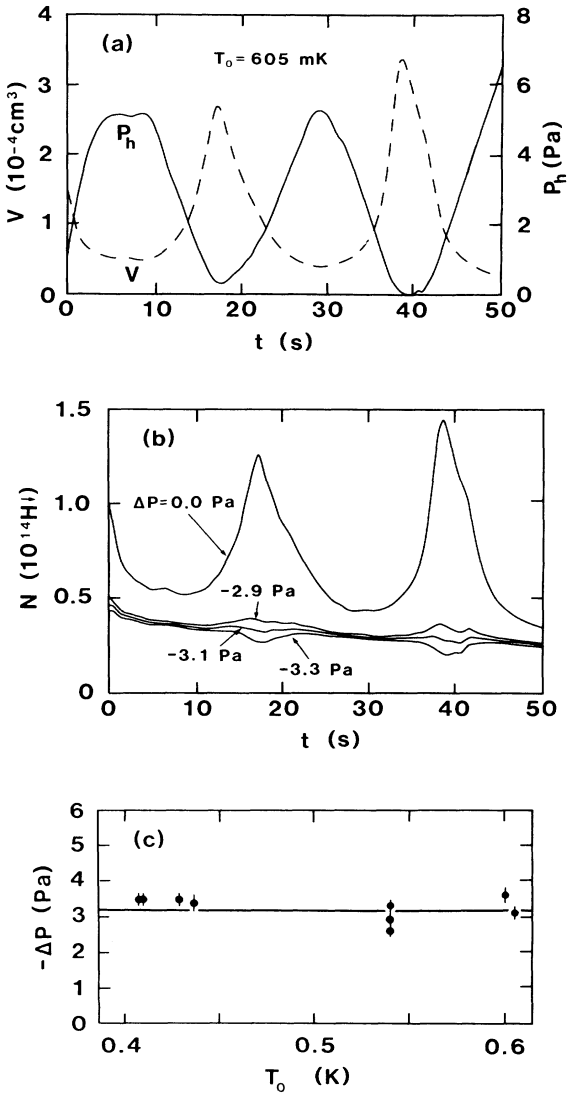

FIG. 3. (a) Compression-decompression cycles at $T_0 = 0.605$ K for H↓ samples larger than the maximum spherical size. Volume V and hydrostatic pressure P_h (as obtained from the level indicator reading) are shown. (b) Total number of H atoms for the data of (a) according to $N = (P + \Delta P)V/k_B T_0$, where $P = P_h + P_s$ and ΔP is a correction (see text). (c) Best ΔP for different values of T_0.

ture T_0. The pressure P is the sum of the hydrostatic pressure P_h and the surface tension pressure P_s of liquid helium ($P=P_h+P_s$; see Sec. IV). The resulting values of PV/k_BT oscillate as shown in Fig. 3(b). We have tried to attribute this nonphysical behavior to errors in the determination of either V or P. However, we have not been able to find a correction of the volume measurement with respect to, e.g., the fringing electric fields of the volume gauge capacitor such that a monotonously decreasing N would result. However, if we assume that the zero of P is off by a constant correction ΔP, we get a monotonously decreasing N with time. This is exemplified by Fig. 3(b) where the best ΔP seems to be -3.1 Pa. The pressure correction $\Delta P(T_0)$ necessary for compression-decompression experiments at different ambient temperatures is given in Fig. 3(c). The mean correction is $\Delta P=-3.2(4)$ Pa. In our earlier report[7] we did not make this correction and even at present the origin of the correction remains unknown. One should notice that the best ΔP is, maybe fortuitously, equal in magnitude to the contribution $\sigma/d=3.2$ Pa to the surface pressure P_s produced by the smaller radius d of a flat cylindrical bubble (cf. Fig. 5). This contribution should not vanish, however, because the wetting angle is zero for a superfluid. Even if P_s ought to be corrected for σ/d, the correction should be applied to flat bubbles only and should vanish once the bubble becomes spherical. However, perhaps due to reasons of volume resolution, we have not been able to verify such a behavior and have therefore subtracted 3.2 Pa from all data obtained for the small SC.

IV. EXTRACTION OF THIRD-ORDER RECOMBINATION RATES

We have analyzed the compression data by fitting decays of bubbles with the help of the following coupled rate equations:

$$
\begin{aligned}
-\dot{N}_a/V &= K_{ab}^{\mathrm{eff}}ab+2K_{aa}^{\mathrm{eff}}a^2+K_{ac}^{\mathrm{eff}}ac+K_{ad}^{\mathrm{eff}}ad+2K_{\mathrm{ex}}(ab^2/3+2a^2b/3+4a^3)\\
&\quad+[(2+\xi_v)K_{bbb}^{v}+(2+\xi_s)K_{bbb}^{\mathrm{eff},s}](ab^2/3+2a^2b/3+a^3)+(K_{aad}a^2+K_{abc}ab/2)(c+d)\\
&\quad+K_{\mathrm{He}}[(2a^2+ab)\epsilon^2+a(c+d)/2](n_{\mathrm{He}}+n_{\mathrm{H}_2})\\
&\quad-G_{ba}(b^2-a^2)+G_{da}[\exp(-2\mu_BB/k_BT)a-d]a-G_{\mathrm{ex}}(bd-ac)\,,\\
-\dot{N}_b/V &= K_{ab}^{\mathrm{eff}}ab+K_{bc}^{\mathrm{eff}}bc+K_{bd}^{\mathrm{eff}}bd+2K_{\mathrm{ex}}(2ab^2/3+a^2b/3-a^3)\\
&\quad+[(2+\xi_v)K_{bbb}^{v}+(2+\xi_s)K_{bbb}^{\mathrm{eff},s}](b^3+2ab^2/3+a^2b/3)\\
&\quad+(K_{bbc}b^2+K_{abc}ab/2)(c+d)+K_{\mathrm{He}}[ab\epsilon^2+b(c+d)/2](n_{\mathrm{He}}+n_{\mathrm{H}_2})\\
&\quad+G_{ba}(b^2-a^2)+G_{cb}[\exp(-2\mu_BB/k_BT)b-c](b+a)+G_{\mathrm{ex}}(bd-ac)\,,\\
-\dot{N}_c/V &= K_{ac}^{\mathrm{eff}}ac+K_{bc}^{\mathrm{eff}}bc-(\xi_vK_{bbb}^{v}+\xi_sK_{bbb}^{\mathrm{eff},s})(b^3+2ab^2/3+a^2b/3)+[K_{bbc}(a^2+b^2)+K_{abc}ab]c\\
&\quad+K_{\mathrm{He}}(a+b)c(n_{\mathrm{He}}+n_{\mathrm{H}_2})/2-G_{cb}[\exp(-2\mu_BB/k_BT)b-c](b+a)-G_{\mathrm{ex}}(bd-ac)\,,\\
-\dot{N}_d/V &= K_{ad}^{\mathrm{eff}}ad+K_{bd}^{\mathrm{eff}}bd-(\xi_vK_{bbb}^{v}+\xi_sK_{bbb}^{\mathrm{eff},s})(ab^2/3+2a^2b/3+a^3)+[K_{aad}(a^2+b^2)+K_{abd}ab]d\\
&\quad+K_{\mathrm{He}}(a+b)d(n_{\mathrm{He}}+n_{\mathrm{H}_2})/2-G_{da}[\exp(-2\mu_BB/k_BT)a-d]a+G_{\mathrm{ex}}(bd-ac)\,,
\end{aligned}
\tag{3}
$$

where $a,\ldots,d$ are the number densities

$$n_{|a\rangle}=N_a/V,\ \ldots,\ n_{|d\rangle}=N_d/V$$

of the different hyperfine states. The probability of the third-order dipole recombination to produce an extra $|c\rangle$ or $|d\rangle$ state atom in the bulk is denoted by ξ_v ($=0.91$) and on the surface by ξ_s ($=0.87$).[9] Because $c,d\ll b$ we can assume that a steady state is reached, where $|c\rangle$ and $|d\rangle$ atoms recombine promptly with $|b\rangle$ atoms. This means that $\dot{N}_c\simeq\dot{N}_d\simeq0$ and that c and d can be calculated. It is obvious that these nonlinear equations include too many parameters to be fitted. On the other hand, we know that some terms in Eqs. (3) are so small that they do not contribute significantly to the decay. Our goal is to extract the third-order dipole recombination rate coefficients K_{bbb}^{v} and K_{bbb}^{s}, which we assume to be independent of temperature. However, it is necessary to use the initial nuclear polarization as an additional fitting parameter. All other recombination (K) and relaxation (G) rate constants are fixed to values given below.

The surface reaction rates have been calculated by assuming a steady-state situation on the surface such that evaporation and sticking rates are equal. This leads to the effective rate constant

$$K_x^{\mathrm{eff},S}=(A/V)K_x^{S}[\beta\lambda_T\exp(E_a/k_TT)]^i\,, \tag{4}$$

where $i=2$ or 3 is the order of the reaction and the correction factor β is

$$\beta\simeq[\langle v(T_1)\rangle S(T_0,T_1)]/[\langle v(T_0)\rangle S(T_0,T_0)]\,. \tag{5}$$

Here S is the sticking probability, $\langle v \rangle$ the mean thermal velocity, T_0 the ambient temperature, and T_1 the temperature of the gas adjacent to the surface. For $T > 0.15$ K, $S \simeq 0.33T$ and we get $\beta \simeq (T_1/T_0)^{3/2}$.[26]

The experimental values of the adsorption energy range from $E_a/k_B = 0.89$ K to 1.15 K.[9,27] The narrow temperature range used in this experiment does not allow an accurate determination of the adsorption energy; thus we will use two different values of E_a in order to illustrate the dependence of the results on this choice: (a) $E_a/k_B = 1.0$ K, which represents the mean for the spread in the experimental values, and (b) $E_a/k_B = 1.15$ K in accord with the choice of Sprik *et al.*[3] Furthermore, we set $K_{ab} = 2.5\times10^{-8}\sqrt{T}/B^2$ cm^2/s (where T is in K and B in T).[3] The intrinsic second-order rate constants K_{ac}, K_{ad}, K_{bc}, and K_{bd} are set equal to $K_{ad} = K_{bc} = 3.9\times10^{-5}\sqrt{T}$ cm^2/s,[28] and $K_{bd} = K_{ac} = (1+\gamma)K_{bc}/2$, where $\gamma = K_{aa}/K_{ab} \simeq 3$ is the mean of the values determined by Sprik *et al.*,[12] Yurke *et al.*,[29] and Statt *et al.*[24]

We assume that the rate constants K_{aac}, K_{aad}, K_{abc}, K_{abd}, K_{bbc}, and K_{bbd} of less significant exchange reactions are equal. [This approximation is already partially used in Eqs. (3).] The more influential third-order exchange recombination rate constant K_{ex} is related to K_{bbc} by $K_{ex} \approx K_{bbc}\epsilon^2$. According to Kagan *et al.*[13] K_{ex} has to be multiplied by a factor, which decreases from 2 to 1 when the magnetic field is increased from 5 to 10 T. We use $K_{bbc} = 3\times10^{-33}$ cm^6/s according to Sprik *et al.*[3]

Recombinations with atoms of saturated ^{4}He vapor as the third bodies are only important for surface temperatures higher than about 0.6 K. However, it may be possible that recombination heat evaporates extra ^{4}He atoms to the bubble. However, those atoms have not been included here. Morrow *et al.*[30] have measured the rate constant of the reaction $H+H+He \rightarrow H_2+He$ to be $K_{He} = 2.8\times10^{-33}$ cm^6/s for unpolarized atomic hydrogen. We use this value for the reaction where the third body is a H_2 molecule. As seen in Eqs. (3), K_{He} is multiplied by ϵ^2 only for the a^2 and ab terms. The background H_2 density is estimated by assuming that all H_2 molecules disappear from the bubble after a certain mean diffusion time. We have not taken into account possible $|c\rangle$ or $|d\rangle$ state atoms produced in collisions of $|b\rangle$ or $|a\rangle$ state atoms with highly excited and hot molecules.[5]

All different relaxation rate constants down from the $|c\rangle$ and $|d\rangle$ states have been calculated recently by Lagendijk *et al.*[31] They found good agreement with the experimental value $G_{cb} = 1.2\times10^{-15}$ cm^3/s.[3,5] This value is used in our analysis also for the far less significant electronic relaxation rate constant G_{da}. The calculated spin-exchange rate constant is $G_{ex} = 3\times10^{-13}$ cm^3/s.[31] All other possible relaxation channels have smaller rate constants[32] and need not be considered here. For the nuclear relaxation rate constant G_{ba} we use the theoretical value[32]

$$G_{ba} \simeq [6.33\times10^{-22}\sqrt{T} + 7.57\times10^{-22}E_{ab}/(k_B\sqrt{T})] \times (1+16.68/B)^2 \text{ cm}^3/\text{s} , \quad (6)$$

which is in excellent agreement with the experimental results of Bell *et al.*[5] Here E_{ab} is the energy difference between the two lowest hyperfine states, $E_{ab}/k_B \simeq (34.1+2.04B)$ mK.

Also the shape and temperature of the bubble have to be considered for the analysis. During compression the bubble transforms from a pancake-shaped disk to near spherical shape as sketched in Fig. 4. Because the capillary constant $\sqrt{(2\sigma/\rho g)} = 0.074$ cm of liquid ^{4}He is much larger than the height $2d = 0.022$ cm of the small SC, and the wetting angle is zero, the shape of the meniscus of a flat bubble is nearly a semicircle with the radius d. Here $\sigma = 3.54\times10^{-4}$ N/m is the surface tension[33] and ρ the density of liquid ^{4}He.

We assume that only a fraction f of the surface recombination heat is dissipated in the bubble while the rest is dumped directly in the liquid helium bath. Here we use a "geometrical" fraction $f = 0.5$. This fraction and the volume recombination heat are assumed to be distributed homogeneously over the volume V of the bubble. Because the shortest dimension of the bubble is of order ten times the mean free path, heat is expected to flow out of the gas by normal heat conduction in a viscous medium. We use the thermal conductivity calculated by Lhuillier,[17] which depends on nuclear polarization but is almost independent of temperature in the interval from 0.2 K to 0.7 K. Assuming that the top and bottom surfaces of the bubble are thermally well grounded, the thermal distribution in a large disk-shaped bubble simplifies to a temperature gradient in the vertical direction only. With the notations of Fig. 5 the area of the bubble is $A = 2\pi R^2 + 2\pi^2 Rd + 4\pi d^2$. The temperature distribution is given by

$$T(x) = T_1 + [Q/(2V\kappa e)](d^2 - x^2) , \quad (7)$$

where Q is the recombination heating power; $\kappa \simeq 3.6$ mW/K m is the thermal conductivity;[17] $e = 3$, 2, and 1, respectively, for a sphere ($R = 0$), a toroid, and two parallel planes ($R \gg d$); and x is a distance measured from the center of the sphere or the toroid cylinder or from the midplane between the two parallel planes. The

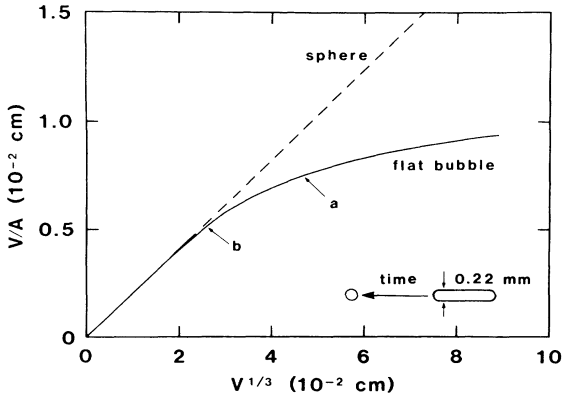

FIG. 4. Volume-to-area ratio for a flat (and eventually spherical) bubble as a function of $V^{-1/3}$. Points a and b mark, respectively, the first and last V/A ratio for the volume decay fitted in Fig. 7.

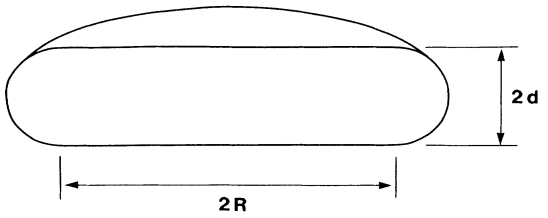

FIG. 5. Flat bubble: height $=2d$ and horizontal diameter $=2R+2d$.

temperature profile in a flat bubble is calculated by using the weighted value

$$e=[(2\pi R^2)\times 1+(2\pi^2 Rd)\times 2+(4\pi d^2)\times 3]/A \ .$$

Thus the vertical temperature gradient in a large disk-shaped bubble reduces smoothly to a radial one as $R\rightarrow 0$. Because Q is temperature dependent, $T(x)$ and Q have to be calculated self-consistently for any given pressure. We have estimated the Kapitza temperature jump $\Delta T=T_1-T_0$, by using the definition of the thermal accommodation coefficient α, which yields the relation

$$Q=\alpha(T_1)(nv/4)A\,2k_B\Delta T \ . \tag{8}$$

As the experimental values of α (Refs. 34 and 35) agree well with the calculated results of Statt,[36] we have used the latter ones to calculate ΔT.

The gas pressure inside the H↓ bubble is balanced by the hydrostatic pressure P_h of the liquid ^{4}He column and the surface pressure

$$P_s\approx\sigma[(R+d)^{-1}+d^{-1}] \ ,$$

where $R+d$ is the horizontal radius of the disk-shaped bubble (Fig. 5). For the larger SC, the height of the AS is larger than the capillary constant and the surface pressure is calculated by minimizing the total free energy

$$\int \sigma\, dA+\int \rho g z\, dV$$

with the constraint $\int dV=\text{const.}$[37] The results are shown in Fig. 6. The correction to the measured hydrostatic pressure by the upward force, which the magnetic field gradient exerts on the diamagnetic ^{4}He column in the level gauge, is usually less than 2% for our magnetic field profile.[38]

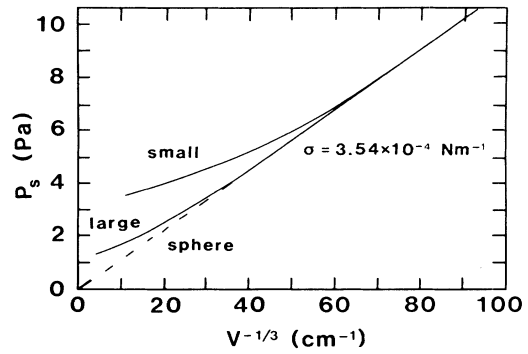

FIG. 6. Volume dependence of surface tension pressure for bubbles in the small and the large sample cells. The surface tension $\sigma=3.54\times 10^{-4}$ N/m (Ref. 33) has been used.

In order to find the rate constants K^v_{bbb} and K^s_{bbb} from the compression data, when all other parameters are assumed to be known, the following fitting procedure was used: At time $t=t_0$ the nuclear polarization is chosen such that it produces the observed initial slope of the volume decay. In later iterations only P and T_0 data are used to calculate a new volume $V(t)$, which is then compared with the measured volume $V_m(t)$. The best fitting parameters K^v_{bbb} and K^s_{bbb} minimize

$$S^2(t)=\left[\sum_i[(V-V_m)^2/V_m]dt_i\right]\Big/(t_0-t) \ .$$

Figure 7(a) shows a typical volume decay fit at the ambient temperature $T_0\simeq 0.53$ K and $B=6.0$ T. In addition to the temperatures T_0 and T_1 the calculated time evolution of the temperature $T_m=T(0)$ in the center of the bubble is also shown for this fit in Fig. 7(b). In the course of compression the temperature difference T_m-T_0 is seen to increase slowly. It is about 20 mK most of the time and 50 mK at the end of the fit. Figure 4 shows that also the A/V ratio changes in this case from 130 cm^{-1} (point *a*) to 190 cm^{-1} (point *b*).

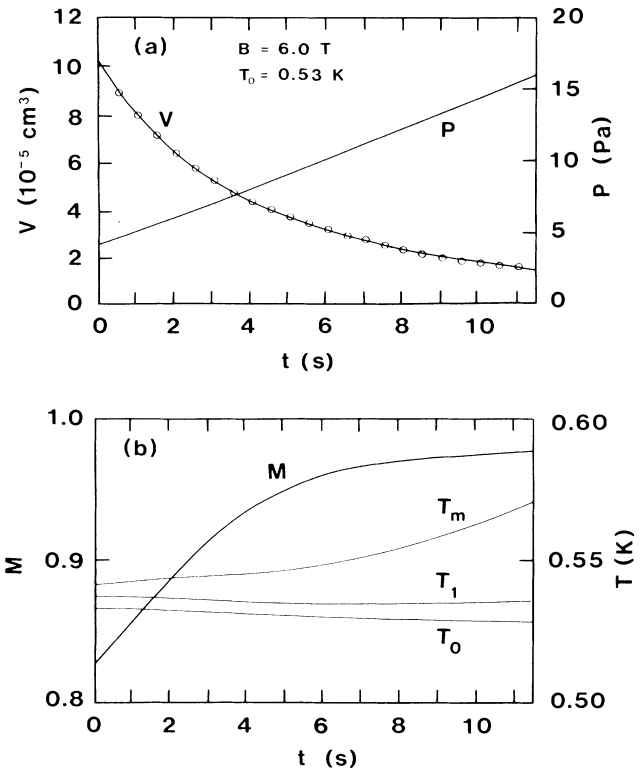

FIG. 7. Typical fit to decaying volume during a compression sweep at $T_0\simeq 0.53$ K and $B=6.0$ T. (a) Volume V and total pressure P. (b) Time evolutions of average nuclear polarization M, ambient temperature T_0, temperature T_1 in gas adjacent to bubble surface, and temperature T_m of the bubble center.

Obviously, reliable values of both bulk and surface recombination rate constants cannot be extracted from the analysis of a single compression experiment, because different combinations of K^v_{bbb} and K^s_{bbb} give good fits to the $V_m(t)$ data. Therefore we have analyzed several tens of compression sweeps at different ambient temperatures T_0 and fitted the data by using the effective dipole rate constant $K_d^{\rm eff}$. Figure 8 shows $K_d^{\rm eff}$ as a function of $1/T_0$ for four magnetic fields. In keeping with Eqs. (1) and (4), we can write

$$K_d^{\rm eff} \simeq K^v_{bbb} + X(T_0) K^s_{bbb} ,$$

where

$$X(T) = (A/V)[\beta \lambda_T \exp(E_a/k_B T)]^3 .$$

During compression A/V changes, but because V varies only slowly with time during the last stage of the compression [cf. Fig. 7(a)], where the recombination rate is most sensitive to $K_d^{\rm eff}$, we can take an A/V value close to the end of the fit to represent the whole sweep. Both K^v_{bbb} and K^s_{bbb} are now found by plotting $K_d^{\rm eff}$ as a function of X (Fig. 9). The field dependence of these constants remains yet unresolved due to the limited number of data points per field value and their large scatter.[39] On the basis of the present work one is unable to judge whether the rate constants decrease with B as has been observed,[4,16] or increase as the theory[13,40] predicts.

The fact that the nuclear polarization M is assumed to be constant throughout the bubble can be regarded as one of the weak points of the above analysis. Due to the second-order surface recombination, close to the surfaces M is likely to be higher there than in the center of the bubble. As exemplified by Fig. 7(b) the average polarization evolves quite rapidly towards a nearly constant value, which is better than 95% for the analyzed compressions. The homogeneous distribution of heat assumed here should give an upper limit to the temperature of the gas and thus a lower limit to the density and so we should get an upper bound to the bulk recombination constant K^v_{bbb}.

As seen from the intercepts displayed in Figs. 9(a) and 9(b) the value for K^v_{bbb} is 2.0×10^{-39} cm^6/s or $2.7(7)\times10^{-39}$ cm^6/s, depending on whether E_a is chosen to be 1.0 K or 1.15 K, respectively. These values are in good agreement with the experimental results $K^v_{bbb}=2.0(5)\times10^{-39}$ cm^6/s at $B=9.8$ T by Sprik *et al.*[3] and $2.3(2)\times10^{-39}$ cm^6/s at 7.6 T by Bell *et al.*[5] The theoretical values $K^v_{bbb}\approx4\times10^{-39}$ cm^6/s and 4.3×10^{-39} cm^6/s for 10 T have been reported, respectively, by Kagan *et al.*[13] and de Goey *et al.*[40] Our average third-order dipole recombination rate constants on the surface are $K^s_{bbb}=1.0\times10^{-24}$ cm^4/s and $8(2)\times10^{-25}$ cm^4/s, when $E_a=1.0$ K and 1.15 K, respectively. These values are about twice as large as the experimental results

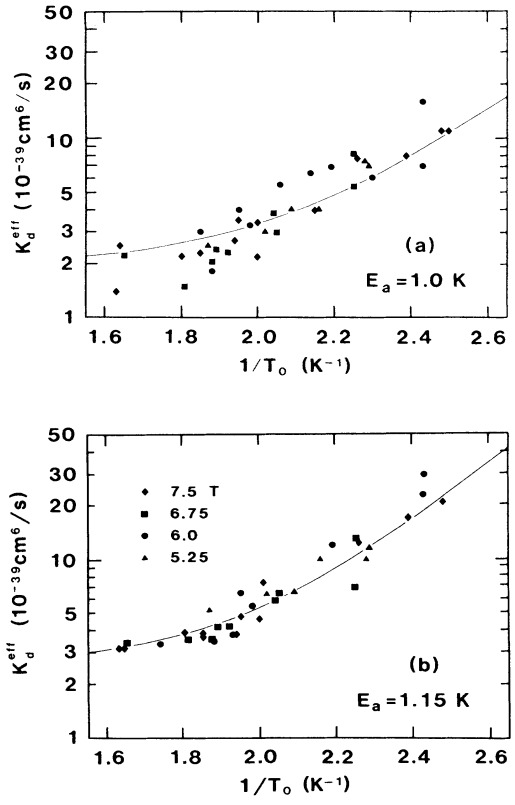

FIG. 8. Fitted effective third-order dipole recombination rate constant $K_d^{\rm eff}$ as a function of $1/T_0$ for different fields (a) $E_a=1.0$ K and (b) $E_a=1.15$ K.

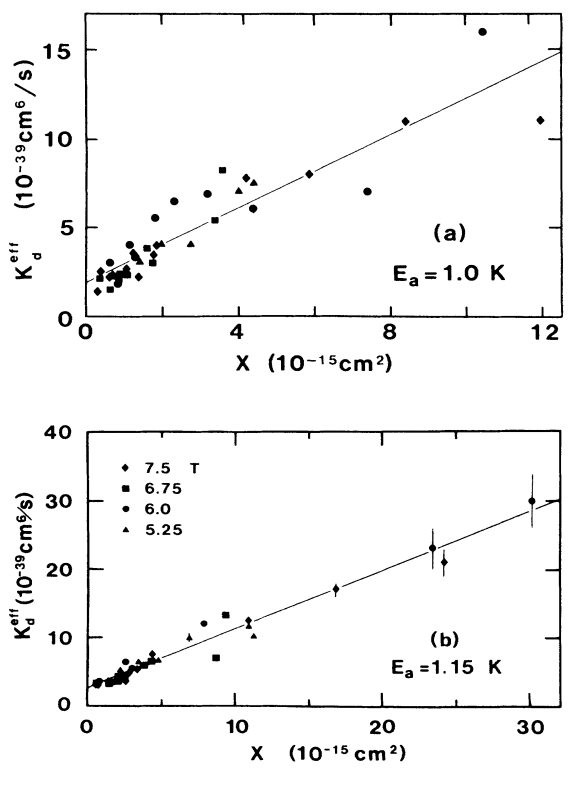

FIG. 9. $K_d^{\rm eff}$ of Fig. 8 as a function of $X\simeq(A/V)[\beta\lambda_T\exp(E_a/k_BT_0)]^3$ where $\beta\approx(T_1/T_0)^{3/2}$. (a) $E_a=1.0$ K and (b) $E_a=1.15$ K.

$K^s_{bbb}=3.1(1)\times10^{-25}$ cm^4/s at 7.6 T by Bell *et al.*[5] and $3.9(1)\times10^{-25}$ cm^4/s at 8 T by Sprik *et al.*,[16] while the theoretical value $K^s_{bbb}=6.6\times10^{-26}$ cm^4/s of de Goey *et al.*[40] is smaller by more than an order of magnitude. The variation in the fitted results depending on the choice for the adsorption energy is surprisingly small. The reason for this is that a change in E_a is apparently to a large degree compensated by a corresponding adjustment in the value of the initial polarization. The fact that the third-order dipole recombination rate constants observed in the present work are larger than earlier ones might be attributed in part to the nonthermal enhancement of recombination suggested by Bell *et al.*[5] One should point out that the fitting procedure involves samples with densities exceeding 10^{18} cm^{-3}, where this enhancement is expected to play a role.[5]

Comparing Figs. 9(a) and (b) it is evident that the choice $E_a=1.15$ K gives a better linear fit with a smaller scatter. Note that one should compare these figures scaled as they are shown, since X depends exponentially on $3E_a$. Note also that both figures include the data from the temperature range shown in Figs. 8(a) and 8(b). The difference between these two cases is further clarified by comparing fits for K^s_{bbb} once K^v_{bbb} has been fixed to one of the values found above. This analysis gives a roughly 4 times smaller standard deviation for the fitted K^s_{bbb} value when $E_a=1.15$ K than when $E_a=1.0$ K. Thus the choice $E_a=1.15$ K appears to be preferable, although $E_a=1.0$ K is more in line with the most recent experiments.[5,41,42]

V. EXPLOSIONS

The phenomenon of thermal explosion of compressed H↓ bubbles in liquid ^{4}He was first observed[2] for relatively large samples at $T/B>0.1$ K/T. It was associated with the electronic $|b\rangle\rightarrow|c\rangle$ relaxation which is accelerated exponentially with increasing T/B. Here we investigate this explosive behavior as a function of the parameters T_0, V, B, M, and dP_h/dt. Measured explosion pressures P_c are shown in Fig. 10 for two narrow ranges of volume V and magnetic fields $B=4.5$–7.5 T as a function of the ambient temperature T_0. As shown in Fig. 11, P_c seems to depend only slightly on the compression rate dP_h/dt. However, a relatively large dP_h/dt is required to reach the conditions leading to explosive recombination in a small bubble in high fields and at high temperature. This is understandable, because the recombination lifetime τ of a small bubble at high density is short (e.g., $\tau=n/\dot{n}\approx10$ s for $n=3\times10^{18}$ cm^{-3} at $T\approx0.5$ K). For small dP_h/dt the necessary high pressure for the explosion can be generated by the surface pressure, but in this case the bubble may already be smaller than our volume detection limit before it explodes. In some cases no explosion at all could be detected, possibly due to a vanishingly small number of atoms left in the bubble. On the other hand, large samples sometimes exploded at low pressure (see Figs. 13 and 14) even with low dP_h/dt.

We next consider a model for thermal explosions based on the work of Kagan *et al.*[20] who examined,

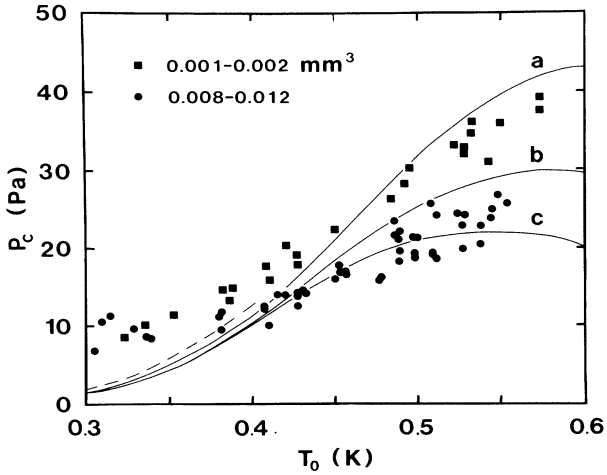

FIG. 10. Onset pressure P_c for thermal explosion as a function of T_0 for two ranges of spherical sample volumes in magnetic fields 4.5–7.5 T. The curves represent the calculated P_c for (a) $V=1.5\times10^{-6}$ cm^3 and $B=6.0$ T, (b) 10^{-5} cm^3 and 6.0 T, and (c) 10^{-5} cm^3 and 5.25 T. The recombination heat is assumed to be distributed homogeneously inside the bubble volume, except in the case of the dashed line, where half of the surface recombination heat is (other parameters being as for curve a) assumed to be dumped directly into the liquid He bath ($f=0.5$).

however, H↓ gas between two infinite parallel planes and ignored surface recombinations. Here we concentrate on the case of a spherical H↓ immersed in bulk liquid helium. Almost all atoms are in the gas phase so that by integrating over the volume V the total atom number N is obtained as

$$N=\frac{4\pi P}{k_B q}\left[\frac{\left[\frac{T_1}{q}+r^2\right]^{1/2}}{2}\ln\frac{\left[\frac{T_1}{q}+r^2\right]^{1/2}+r}{\left[\frac{T_1}{q}+r^2\right]^{1/2}-r}-r\right], \tag{9}$$

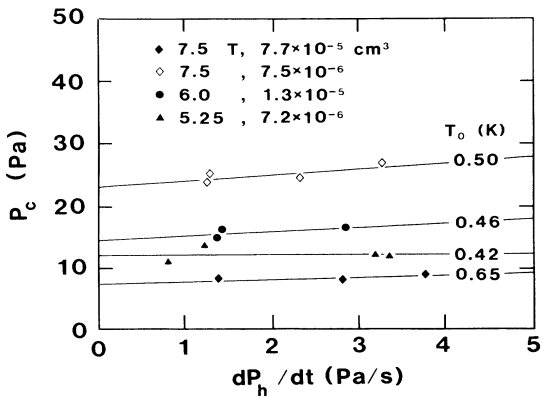

FIG. 11. Compression rate dependences of the explosion pressure.

where r is the bubble radius and $q=Q/(6VK)$. For constant V two values of P satisfy Eq. (9). Only the lower pressure corresponds to a physically acceptable case. These two solutions approach each other as N increases and meet at a single pressure $P_c=P(N_c)$ above which no solution exists. This point is interpreted as the thermal explosion pressure P_c, where $dT/d\langle n\rangle\rightarrow\infty$. During compression N decreases, but so does V, and finally the explosion condition is reached.

Calculated explosion pressures for the volumes 0.01 and 0.0015 mm^3 and magnetic fields 6 and 5.25 T are shown in Fig. 10. The H-H interactions on the surface[15] have been included in the calculation of the surface density. The polarization M at the explosion moment has been estimated from a fitting procedure described in Fig. 7(b). As T_0 increases from 0.4 to 0.6 K, M decreases from about 99% to 95%. The solid curves in Fig. 10 have been calculated under the assumption that all recombination heat is distributed into the gas ($f=1$). However, in some cases the excited H_2^* molecules might not have enough time to relax to the ground state before leaving the bubble. If one assumes $f=0.5$, P_c grows as shown by the dashed curve of Fig. 10. At low temperatures the third-order surface recombination heat turns out to be far more important for the explosions than the electronic $|b\rangle\rightarrow|c\rangle$ relaxation. The latter plays a significant role in triggering explosions and decreasing P_c at higher temperatures. However, at temperatures of 0.5 K or above the calculated magnetic field dependence of P_c is larger than the measured one (cf. Figs. 10 and 12).

As shown in Fig. 10, at low T_0 the observed explosion pressures are significantly higher than those predicted by the explosion model. As yet we do not have a satisfactory explanation for this discrepancy, but it should be kept in mind that, due to the long thermal path between the bubble and the bolometer carbon, the measured T_0 can be lower than the actual temperature of the adsorbed H↓. The total thermal impedance to the transfer of the recombination heat includes liquid helium, Kapton and gold foils, and the thermal boundary resistances. It is also possible[43] that the surface layer is not in thermal equilibrium with liquid ^{4}He due to a weak ripplon-H coupling.[44] This would mean a reduced surface density and consequently decreased recombination heating allowing a higher P_c.

At higher T_0 the explosions occur at lower pressures than expected on the basis of the simple model. As mentioned above, the uniform polarization M used in this analysis is too high and thus leads to an overestimate of P_c. According to our experiments and the model, P_c goes through a maximum as a function of T_0, but as shown in Figs. 13 and 14, the data decrease far more rapidly with increasing T_0 than the model predicts. The data of Fig. 13 have been taken in the small SC, while Fig. 14 corresponds to the large SC. The premature explosion of the large bubbles at $T_0>0.45$ K (Fig. 14) may be attributed to a low M developed during a short interval between the beginning of the compression and the explosion. As shown in Fig. 14 this would, however, require that for $B=6$ T polarization is close to zero and for $B=4.5$ T about 50%. The same explanation can be offered for the high-temperature data of Fig. 13, but less convincingly. Therefore, the possibility of the nonthermalized recombination energy leading to a direct depolarization of H↓ atoms to the electronic spin-reversed states[5] should be considered. Unfortunately, no quantitative estimates for the relevant enhancement factor of the $|b\rangle\rightarrow|c\rangle$ relaxation process have yet been proposed.

The volume dependence of the explosion pressure is shown in Fig. 15, where the straight lines are least-square fits to the data of the form $P_c\propto V^{-1/\nu}$. For $T_0=0.54$ K the fit gives $\nu\approx3.2$ and for $T_0=0.32$ K one obtains $\nu\approx8.6$. The thermal explosion model predicts $\nu=3$, 4.5, 6, and 9, when the explosion is driven by

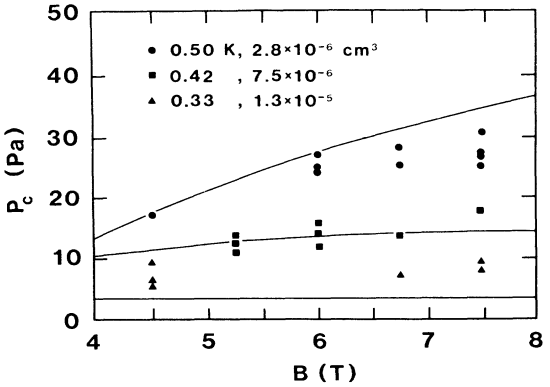

FIG. 12. Magnetic field dependence of the explosion pressure for a few constant temperatures and sample volumes. The curves have been calculated according to the thermally activated explosion model.

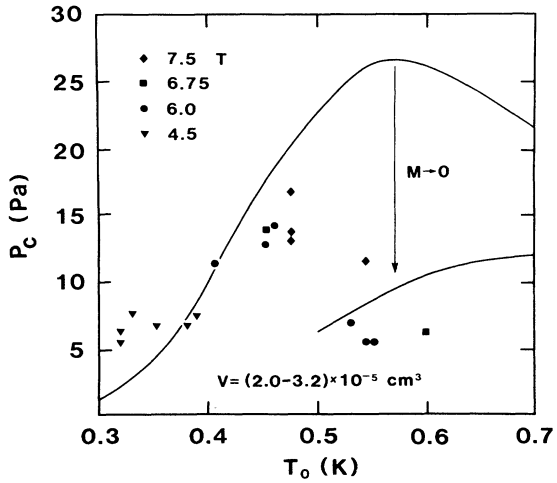

FIG. 13. Explosion pressure as a function of T_0 for $V=(2.0-3.2)\times10^{-5}$ cm^3. The upper solid curve represents the calculated P_c for $V=2.6\times10^{-5}$ cm^3, $B=6.0$ T, and a nuclear polarization M taken to be the final value reached in the volume-decay analysis [cf. Fig. 7(b)]. The lower curve at high T_0 shows how the calculated P_c changes when M decreases to zero.

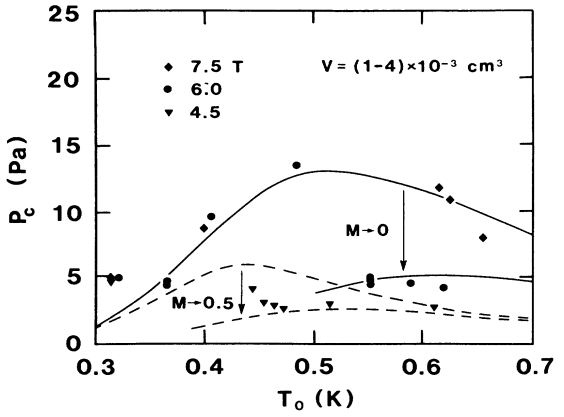

FIG. 14. Explosion pressure observed in the large sample cell at different T_0 for samples with $V=(1-4)\times10^{-3}$ cm^3. The upper solid curve has been calculated for $V=2.5\times10^{-3}$ cm^3, $M=98\%$, and $B=6.0$ T, while in the case of the upper dashed curve the field has been decreased to $B=4.5$ T. The lower curves at high T_0 represent the corresponding cases but with $M=0$ (solid curve) or $M=50\%$ (dashed curve).

second-order volume, third-order volume, second-order surface, or third-order surface recombination, respectively.

Sometimes explosions have been observed several seconds after the bubble has become smaller than the resolution limit 10^{-6} cm^3 of the volume gauge. If we use the surface tension pressure $P_s=11.4$ Pa for $V=10^{-6}$ cm^3, we find that our highest $P_h=47.6$ Pa at explosion, observed at $T_0=0.54$ K and $B=7.5$ T, corresponds to $P_c>59$ Pa. It is estimated that $T_1\approx0.6$ K, which gives a lower limit of about 7×10^{18} cm^{-3} to the H↓ density next to the bubble surface. Due to the steep temperature gradient in the bubble the average density $\langle n\rangle$ is naturally smaller. We estimate $\langle n\rangle\approx5\times10^{18}$ cm^{-3} and the temperature of the bubble center to reach $T_m\approx1.2$ K.

We have observed that adding ^{3}He to the ^{4}He piston

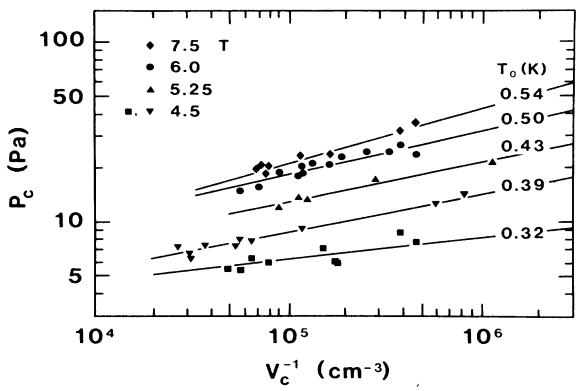

FIG. 15. Volume dependence of the explosion pressure at different constant temperatures and fields. The straight lines are least-square fits to the data.

rather decreases than increases P_c in the present range of temperatures. The increased gas density in the bubble due to the presence of the ^{3}He vapor leads to enhanced volume recombination and the dissolved ^{3}He in the He bath lowers its thermal conduction. At lower temperatures below 0.2 K a ^{3}He coating would be formed on the surface of ^{4}He,[27] which would reduce the binding energy E_a of H↓ by a factor of about 3.[9,28] Consequently, P_c could become roughly 20-fold, because for low temperatures, where surface recombination dominates, $P_c\propto\exp(-3E_a/2k_BT)$ [cf. Eq. (10)]. The maximum n_c reported above for H↓ at $T_1\approx0.6$ K was obtained in the temperature regime where n_c comes closest to the BEC limit, but even this density is by a factor of 35 smaller than the corresponding $n_{\rm BEC}$. For the average conditions of the bubble $\langle n_c\rangle\approx0.01n_{\rm BEC}$.

We next examine prospects for achieving conditions required for the two-dimensional superfluid transition of the Kosterlitz-Thouless (KT) type in the H↓ monolayer adsorbed on the surface of a compressed H↓ bubble. The saturation density of the adsorbed surface layer is given by

$$n_s^{\rm sat}=E_a/2u_s+u_0n/u_s\ ,$$

where $u_0\approx4.4\times10^{-22}$ K cm^3 and $u_s\approx4.1\times10^{-15}$ K cm^2 are the nearest-neighbor interaction energies in the bulk and on the surface, respectively.[45] At low temperatures ($k_BT<E_a$) the adsorption isotherms approach $n_s^{\rm sat}$ at lower and lower build densities with $n_s^{\rm sat}\approx1.2\times10^{14}$ cm^{-2} for a ^{4}He surface ($E_a=1.0$ K) and 0.41×10^{14} cm^{-2} for a ^{3}He surface ($E_a=0.34$ K).[9] In these conditions the density required for the Kosterlitz-Thouless transition $n_{\rm KT}\approx2mk_BT_0/\pi\hbar^2$ is some fraction of the saturation value $n_s^{\rm sat}$, typically of order 0.1–0.5, and will be reached at low bulk density well below the BEC limit. Furthermore, if the mean free path of H↓ atoms remains comparable with the dimensions of the bubble, the recombination energy is mainly dissipated in collisions at the surface of the bubble. Then the gas temperature, which may be calculated from Eq. (8), will be nearly constant throughout the bubble. On the basis of the good agreement between the experimental[34,35] and theoretical[36] values of the thermal accommodation coefficient α it can be expected to be well approximated by $\alpha=\alpha_0T\approx0.5T$ to below 0.1 K. Then one easily finds for the explosion density

$$n_c\approx0.38(k_B\alpha_0v_0/fDL_s\lambda_0^3)^{1/2}T_0^2\exp(-3E_a/2k_BT_0)\ , \tag{10}$$

where $v=v_0\sqrt{T}$ is the average thermal velocity of H atoms, fD is the fraction of the surface recombination energy per molecule which is dissipated in the bubble, $L_s=2(1+\xi_s)K_{bbb}^s$ [cf. Eq. (3)], and $\lambda_T=\lambda_0/\sqrt{T}$. By using the measured field dependence of the third-order dipole rate constants[5,16] we extrapolate to the comparatively large field of 15 T and get $L_s\approx1.1\times10^{-24}$ cm^4/s. Since the limiting surface density for the KT transition is

$$n_{\rm KT}\approx2mk_BT_c/\pi\hbar^2\approx1.31\times10^{14}T_0\ {\rm cm}^{-2}$$

(Ref. 46), one gets for $B=15$ T an upper limit to the adsorption energy

$$E_a/k_B \leq 2T_0 \ln(4.47T_0^{1/2}/\sqrt{f}) .$$

For $f=1$ we now obtain the conditions $E_a/k_B \leq 0.16$ K at $T_0=0.15$ K and $E_a/k_B \leq 1.15$ K at $T_0=0.5$ K. The latter rough estimate points to the possibility of achieving the KT phase transition when an extremely small bubble of H↓ is compressed in ^{4}He liquid at $T_0 \approx 0.5$ K. At temperatures less than 0.2 K even the use of ^{3}He would not help. One should also notice that Collaudin *et al.*[43] have pointed out that, in order to display coherent two-dimensional superfluidity, the adsorbed H↓ atoms must have an average residency time clearly longer than the characteristic superfluid correlation time. However, this condition will be fulfilled only at temperatures less than about 0.2 K.[43] The attainment of the transition does not therefore look promising. If, however, $f=0.003$, Eq. (10) gives $E_a/k_B \leq 1.0$ K for $T_0=0.15$ K. It would thus be important to know how the excited hydrogen molecules behave when they hit the liquid helium surface, or more exactly, how probable it is that H_2^* will be dissolved in the liquid.

VI. CONCLUSIONS

We have presented the results from extensive measurements on the third-order (H+H+H) recombination rates and thermal explosion of spin-polarized hydrogen gas compressed to small bubbles inside superfluid liquid helium in the ranges of ambient temperature T_0 from 0.3 to 0.7 K and polarizing field B from 4.5 to 7.5 T. The rate constants extracted for both volume and surface dipole recombination are somewhat larger than those reported previously. We have observed that the explosions limit the highest possible H↓ density in the bubble to values which are more than 1 order of magnitude below the density required for Bose-Einstein condensation. The bubble is driven out of thermal equilibrium and ultimately to an explosive instability by inadequate transfer of recombination heat to the surroundings, when the recombination rate becomes excessive. We find that the onset pressure for explosion, P_c, has a maximum as a function of T_0 and that the maximum P_c increases with decreasing sample volume. Increasing B has been observed to shift the maximum towards higher T_0. Electronic $|b\rangle \rightarrow |c\rangle$ relaxation in the bulk gas can produce a significant field dependence of P_c only at temperatures higher than about 0.5 K. Our model calculation of the thermal explosion process shows that the maximum in P_c is a result of a trade-off between third-order dipole surface recombination at low temperatures and, on the other hand, third-order dipole recombination and $|b\rangle \rightarrow |c\rangle$ relaxation in the bulk gas at higher temperatures. In the vicinity of maximum P_c at $B=7.5$ T we have been able to compress a H↓ bubble with $V<10^{-6}$ cm^3 to a maximum density of about 7×10^{18} cm^{-3}. Toward high temperatures P_c decreases, however, faster than is expected on the basis of the simple model. This cannot only be attributed to incomplete nuclear polarization, but may also be due to enhanced second-order bulk recombination caused by evaporated ^{4}He atoms or to the enhancement of electronic relaxation by nonthermalized recombination heat, especially as the bubble center reaches relatively high temperatures prior to explosion. The compression rate seems to have only a slight, if any, effect on P_c.

We estimate that, even in the challenging experimental conditions of extremely small bubbles (10–20 μm in diameter) and very high fields, only marginal possibilities exist that surface-adsorbed H↓ could be rendered to display two-dimensional superfluidity below a Kosterlitz-Thouless transition. It is therefore believed that Bose-Einstein condensation may not be reached at all by straightforward hydraulic compression.

ACKNOWLEDGMENTS

We wish to thank I. P. Krylov, K. Salonen, S. Penttilä, M. Karhunen, and J. Wallenius for their contributions to this work. We also acknowledge the financial support of the Academy of Finland (Grant No. 09/361).

*Permanent address: Low Temperature Laboratory, Helsinki University of Technology, 02150 Espoo, Finland.

[1] I. F. Silvera and J. T. M. Walraven, Phys. Rev. Lett. **44**, 164 (1980).

[2] R. Sprik, J. T. M. Walraven, and I. F. Silvera, Phys. Rev. Lett. **51**, 479 (1983); **51**, 942(E) (1983).

[3] R. Sprik, J. T. M. Walraven, and I. F. Silvera, Phys. Rev. B **32**, 5668 (1985).

[4] H. F. Hess, D. A. Bell, G. P. Kochanski, R. W. Cline, D. Kleppner, and T. J. Greytak, Phys. Rev. Lett. **51**, 483 (1983).

[5] H. F. Hess, D. A. Bell, G. P. Kochanski, D. Kleppner, and T. J. Greytak, Phys. Rev. Lett. **52**, 1520 (1984); D. A. Bell, H. F. Hess, G. P. Kochanski, S. Buchman, L. Pollack, Y. M. Xiao, D. Kleppner, and T. J. Greytak, Phys. Rev. B **34**, 7670 (1986).

[6] T. Tommila, S. Jaakkola, M. Krusius, K. Salonen, and E. Tjukanov, in *Proceedings of the 17th International Conference on Low Temperature Physics, LT-17,* edited by U. Eckern, A. Schmid, W. Weber, and H. Wühl (North-Holland, Amsterdam, 1984), p. 453.

[7] T. Tommila, S. Jaakkola, M. Krusius, I. Krylov, and E. Tjukanov, Phys. Rev. Lett. **56**, 941 (1986).

[8] T. J. Greytak and D. Kleppner, in *New Trends in Atomic Physics,* edited by G. Grynberg and R. Stora (North-Holland, Amsterdam, 1984), Vol. II, p. 1125.

[9] I. F. Silvera and J. T. M. Walraven, in *Progress in Low Temperature Physics,* edited by D. F. Brewer (North-Holland, Amsterdam, 1986), Vol. X, p. 139.

[10] B. W. Statt and A. J. Berlinsky, Phys. Rev. Lett. **45**, 2105 (1980).

[11] R. W. Cline, T. J. Greytak, and D. Kleppner, Phys. Rev. Lett. **47**, 1195 (1981).

[12]R. Sprik, J. T. M. Walraven, G. H. van Yperen, and I. F. Silvera, Phys. Rev. Lett. **49**, 153 (1982).
[13]Yu. Kagan, I. A. Vartanyantz, and G. V. Shlyapnikov, Zh. Eksp. Teor. Fiz. **81**, 1113 (1981) [Sov. Phys.—JETP **54**, 590 (1981)].
[14]L. P. H. de Goey, T. H. M. v. d. Berg, N. Mulders, H. T. C. Stoof, B. J. Verhaar, and W. Glöckle, Phys. Rev. B **34**, 6183 (1986).
[15]V. V. Goldman and I. F. Silvera, Physica (Amsterdam) **107B**, 505 (1981).
[16]R. Sprik, J. T. M. Walraven, G. H. van Yperen, and I. F. Silvera, Phys. Rev. B **34**, 6172 (1986).
[17]C. Lhuillier, J. Phys. (Paris) **44**, 1 (1983).
[18]Yu. Kagan, G. V. Shlyapnikov, and N. A. Glukhov, Pis'ma Zh. Eksp. Teor. Fiz. **40**, 287 (1984) [JETP Lett. **40**, 1072 (1984)]; V. V. Goldman, Phys. Rev. Lett. **56**, 612 (1986).
[19]W. C. Stwalley, Y. H. Uang, R. F. Ferrante, and R. W. H. Webeler, J. Phys. (Paris) Colloq. **41**, C7-27 (1980).
[20]Yu. Kagan, G. V. Shlyapnikov, and I. A. Vartanyantz, Phys. Lett. **101A**, 27 (1984).
[21]T. Tommila, S. Jaakkola, M. Krusius, K. Salonen, and E. Tjukanov, in *Proceedings of the 17th International Conference on Low Temperature Physics, LT-17,* edited by U. Eckern, A. Schmid, W. Weber, and H. Wühl (North-Holland, Amsterdam, 1984), p. 545.
[22]S. Jaakkola, M. Krusius, S. Penttilä, K. Salonen, E. Tjukanov, T. Tommila, and J. Wallenius, in *Proceedings of the 10th International Cryogenic Engineering Conference, ICEC-10,* Helsinki, 1984, edited by H. Collan, P. Berglund, and M. Krusius (Butterworths, London, 1984), p. 266.
[23]C. T. Van Degrift, Rev. Sci. Instrum. **46**, 599 (1975).
[24]B. W. Statt, A. J. Berlinsky, and W. N. Hardy, Phys. Rev. B **31**, 3169 (1985).
[25]I. Krylov, E. Tjukanov, and T. Tommila (unpublished).
[26]J. J. Berkhout, E. J. Wolters, R. van Roijen, and J. T. M. Walraven, Phys. Rev. Lett. **57**, 2387 (1986).
[27]Because unpurified liquid ^{4}He is used in the SC, the natural abundance 0.1 ppm of ^{3}He could create a monolayer on the surface and thus change the adsorption energy and surface tension. However, in the present temperature range 0.25–0.7 K ^{3}He atoms are dissolved into bulk liquid ^{4}He [D. O. Edwards and W. F. Saam, in *Progress in Low Temperature Physics,* edited by D. F. Brewer (North-Holland, Amsterdam, 1978), Vol. VIIa, p. 285].
[28]A. P. M. Matthey, J. T. M. Walraven, and I. F. Silvera, Phys. Rev. Lett. **46**, 668 (1981).
[29]B. Yurke, J. S. Denker, B. R. Johnson, N. Bigelow, L. P. Levy, D. M. Lee, and J. H. Freed, Phys. Rev. Lett. **50**, 1137 (1983).
[30]M. Morrow, R. Jochemsen, A. J. Berlinsky, and W. N. Hardy, Phys. Rev. Lett. **46**, 195 (1981).
[31]A. Lagendijk, I. F. Silvera, and B. J. Verhaar, Phys. Rev. B **33**, 626 (1986).
[32]J. P. H. W. v. d. Eijnde, Ph. D. thesis, Technical University–Eindhoven, 1984 (unpublished).
[33]M. Iino, M. Suzuki, and A. J. Ikushima, J. Low Temp. Phys. **61**, 155 (1985).
[34]J. Helffrich, M. Maley, M. Krusius, and J. C. Wheatley, Phys. Rev. B **34**, 6550 (1986).
[35]K. Salonen, S. Jaakkola, M. Karhunen, E. Tjukanov, and T. Tommila, in *Proceedings of the 17th International Conference on Low Temperature Physics, LT-17,* edited by U. Eckern, A. Schmid, W. Weber, and H. Wühl (North-Holland, Amsterdam, 1984), p. 543.
[36]B. W. Statt, Phys. Rev. B **32**, 7160 (1985).
[37]L. D. Landau and E. M. Lifshitz, *Fluid Mechanics* (Pergamon, Oxford, 1975).
[38]The homogeneity of our magnet is more than an order of magnitude better than that of the magnet used in Ref. 3.
[39]T. Tommila, Ph. D. thesis, University of Turku, Report Series No. Turku-FTL-D14, 1986 (unpublished).
[40]L. P. H. de Goey, J. P. J. Driessen, B. J. Verhaar, and J. T. M. Walraven, Phys. Rev. Lett. **53**, 1919 (1984).
[41]M. W. Reynolds, I. Shinkoda, W. N. Hardy, A. J. Berlinsky, F. Bridges, and B. W. Statt, Phys. Rev. B **31**, 7503 (1985).
[42]H. P. Godfried, E. R. Eliel, J. G. Brisson, J. D. Gillaspy, C. Mallardeau, J. C. Mester, and I. F. Silvera, Phys. Rev. Lett. **55**, 1311 (1985).
[43]B. Collaudin, B. Hebral, and M. Papoular, J. Phys. (Paris) **47**, 1503 (1986).
[44]D. S. Zimmerman and A. J. Berlinsky, Can. J. Phys. **62**, 590 (1984).
[45]D. O. Edwards and I. B. Mantz, J. Phys. (Paris) Colloq. **41**, C7-257 (1980).
[46]D. O. Edwards, Physica (Amsterdam) **109&110B**, 1531 (1982).